HHS Public Access

Author manuscript

Sci Transl Med. Author manuscript; available in PMC 2015 April 22.

Published in final edited form as:

Sci Transl Med. 2014 October 1; 6(256): 256ra135. doi:10.1126/scitranslmed.3009278.

Histone deacetylase inhibition rescues structural and functional brain deficits in a mouse model of Kabuki syndrome

Hans T. Bjornsson[1,2,*,†], **Joel S. Benjamin**[1,3,†], **Li Zhang**[1], **Jacqueline Weissman**[1,4], **Elizabeth E. Gerber**[1], **Yi-Chun Chen**[1], **Rebecca G. Vaurio**[4], **Michelle C. Potter**[5], **Kasper D. Hansen**[1,6], and **Harry C. Dietz**[1,7,8]

[1]McKusick-Nathans Institute of Genetic Medicine, Johns Hopkins University School of Medicine, Baltimore, MD 21205, USA

[2]Department of Pediatrics, Johns Hopkins University School of Medicine, Baltimore, MD 21205, USA

[*]Corresponding author. hbjorns1@jhmi.edu.
[†]These authors contributed equally to this work.

Author contributions: This project was conceived and designed by H.T.B. and H.CD. Illustrations were designed by H.T.B. and H.C.D. Genotyping assay and real-time PCR and analysis were performed by H.T.B. Immunoblot and mouse perfusions were run by L.Z. and J.S.B. Gene trap integration site was mapped by L.Z. Cryosectioning, immunofluorescence, granule cell layer area, and EdU were performed by J.S.B. Confocal microscopy was done by J.S.B., E.E.G., and H.T.B. Epigenetic indicator alleles were conceived by H.T.B. and H.CD. and created by H.T.B., and all cellular and flow cytometry work was done by L.Z. and H.T.B. Drug gavaging was performed by Y.-C.C. Morris water maze, novel object recognition, and open field behavioral tests were run by J.S.B., with fear conditioning and grip strength tests run by H.T.B. Behavioral tests were selected and analyzed by M.C.P., H.T.B., and J.S.B. Drug trials and mouse colony were managed by J.S.B. ChIP-seq was performed by LZ. and analyzed by K.D.H. Neuropsychological analyses were performed by J.W. and R.G.V. The paper was written and formatted by H.T.B., H.CD., and J.S.B. with input from M.CP.

Competing interests: H.T.B. and H.CD. have two provisional patents relevant to this work: “Genetically encoded histone reporter allele constructs,” JHU Ref. No. C12259, and “Methods for treating Mendelian disorders of the epigenetic machinery,” JHU Ref. No. C13033. The other authors declare they have no competing interests.

SUPPLEMENTARY MATERIALS

www.sciencetranslationalmedicine.org/cgi/content/full/6/256/256ra135/DC1

Materials and Methods

Fig. S1. Integration site of gene trap in the *Kmt2d*$^{\beta Geo}$ allele.

Fig. S2. *Kmt2d*$^{+/\beta Geo}$ mice show overlapping phenotypic features with patients with Kabuki syndrome.

Fig. S3. *Kmt2d*$^{+/\beta Geo}$ mice have context-related memory defects.

Fig. S4. *Kmt2d*$^{+/\beta Geo}$ mice show no deficit in flag trial.

Fig. S5. Assessment of motor function in *Kmt2d*$^{+/\beta Geo}$ and *Kmt2d*$^{+/+}$ mice.

Fig. S6. Escape latencies during Morris water maze training.

Fig. S7. H3K4me3 is decreased in the pyramidal layer in *Kmt2d*$^{+/\beta Geo}$ mice compared to *Kmt2d*$^{+/+}$littermates.

Fig. S8. Body and brain size in *Kmt2d*$^{+/\beta Geo}$ mice.

Fig. S9. EdU incorporation.

Fig. S10. Decreased dendrites in DCX^{+} cells in the granule cell layer of *Kmt2d*$^{+/\beta Geo}$ mice.

Fig. S11. Staining for activated caspase 3 does not reveal increased apoptosis in the granule cell layer of *Kmt2d*$^{+/\beta Geo}$ mice compared to *Kmt2d*$^{+/+}$ littermates.

Fig. S12. HDAC3 attenuates signal of the H4ac indicator.

Fig. S13. Both indicators demonstrate a deficiency in *Kmt2d*$^{+/\beta Geo}$ mice.

Fig. S14. Improved H3K4 trimethylation activity in *Kmt2d*$^{+/\beta Geo}$ cells transiently transfected with H3K4 trimethylation indicator and treated with MS275.

Fig. S15. In vivo responses to AR-42.

Fig. S16. AR-42–induced expression of a known KMT2D target gene.

Fig. S17. MA plots indicate a shift in the balance of H3K4me3 upon treatment with AR-42.

Fig. S18. A visualization of shifts in balance between the two states (genotype or AR-42) as a function of intensity demonstrates an abnormality in *Kmt2d*$^{+/\beta Geo}$ that is responsive to AR-42.

Fig. S19. Serum control experiments for antibodies used for immunofluorescence.

Table S1. A summary of genotypes, drugs, and quality measures of ChIP-seq experiments. References (52, 53)

[3]Predoctoral Training Program in Human Genetics, McKusick-Nathans Institute of Genetic Medicine, Johns Hopkins University School of Medicine, Baltimore, MD 21205, USA

[4]Kennedy Krieger Institute, Baltimore, MD 21205, USA

[5]Brain Science Institute, Neurology Department, Johns Hopkins University School of Medicine, Baltimore, MD 21205, USA

[6]Department of Biostatistics, Bloomberg School of Public Health, Baltimore, MD 21205, USA

[7]Division of Pediatric Cardiology, Department of Pediatrics, Johns Hopkins University School of Medicine, Baltimore, MD 21205, USA

[8]Howard Hughes Medical Institute, Baltimore, MD 21205, USA

Abstract

Kabuki syndrome is caused by haploinsufficiency for either of two genes that promote the opening of chromatin. If an imbalance between open and closed chromatin is central to the pathogenesis of Kabuki syndrome, agents that promote chromatin opening might have therapeutic potential. We have characterized a mouse model of Kabuki syndrome with a heterozygous deletion in the gene encoding the lysine-specific methyltransferase 2D (*Kmt2d*), leading to impairment of methyltransferase function. In vitro reporter alleles demonstrated a reduction in histone 4 acetylation and histone 3 lysine 4 trimethylation (H3K4me3) activity in mouse embryonic fibroblasts from $Kmt2d^{+/\beta Geo}$ mice. These activities were normalized in response to AR-42, a histone deacetylase inhibitor. In vivo, deficiency of H3K4me3 in the dentate gyrus granule cell layer of $Kmt2d^{+/\beta Geo}$ mice correlated with reduced neurogenesis and hippocampal memory defects. These abnormalities improved upon postnatal treatment with AR-42. Our work suggests that a reversible deficiency in postnatal neurogenesis underlies intellectual disability in Kabuki syndrome.

INTRODUCTION

Kabuki syndrome is an autosomal dominant condition caused by heterozygous loss-of-function mutations in either of two genes (1–3) with complementary functions: lysine-specific methyltransferase 2D (*KMT2D*) on human chromosome 12 or lysine-specific demethylase 6A (*KDM6A*) on human chromosome X. KMT2D is a methyltransferase that adds a trimethylation mark to H3K4 (H3K4me3, an open chromatin mark), whereas KDM6A is a demethylase that removes trimethylation from histone 3 lysine 27 (H3K27me3, a closed chromatin mark). Both genes facilitate the opening of chromatin and promote gene expression (1–3). It is therefore likely that the observed gene dosage sensitivity in Kabuki syndrome, despite the apparent redundancy of the H3K4 trimethylation machinery, involves a relative imbalance between open and closed chromatin states for critical target genes. If this is the case, it may be possible to restore this balance with drugs that promote open chromatin states, such as histone deacetylase inhibitors (HDACi). To test this hypothesis, we have characterized a mouse model of Kabuki syndrome with a heterozygous mutation in *Kmt2d* that results in replacement of the SET (suvar, enhancer of zeste, trithorax) methyltransferase domain ($Kmt2d^{+/\beta Geo}$) by a β-Geo cassette. $Kmt2d^{+/\beta Geo}$ mice have

hippocampal memory defects that correlate with multiple abnormalities in the granule cell layer of the dentate gyrus, a prominent site of adult neurogenesis (4, 5). Guided by the results of in vitro analyses using reporter alleles that monitored histone 4 (H4) acetylation and H3K4 trimethylation in cells derived from Kabuki syndrome mice, we find that oral administration of the HDACi AR-42 to either young (1- to 2-month-old) or adult (5- to 6-month-old) *Kmt2d*$^{+/\beta Geo}$ mice normalized both structural and functional deficits in the dentate gyrus in association with restoration of H3K4 trimethylation.

RESULTS

Kmt2d$^{+/\beta Geo}$ mice

KMT2D is a member of the mixed lineage leukemia (MLL) family of *Drosophila* trithorax orthologs that is encoded on human chromosome 12 and mouse chromosome 15. An alternative name for *KMT2D* is mixed lineage leukemia 2 (*MLL2*). All members of this family contain a SET domain, which confers the H3K4 methyltransferase activity, as well as other domains (6) that delineate individual functions (Fig. 1A). A mouse model harboring a loss-of-function allele for *Kmt2b*, encoded on human chromosome 19 and mouse chromosome 7, has been characterized previously (7), demonstrating hippocampal memory defects. This gene has been alternatively designated *Mll4* or *Mll2*, leading to confusion in the literature regarding nomenclature for this particular gene family, as discussed in a recent publication by Bögershausen *et al*. (8). To specifically assess the underlying pathogenesis of Kabuki syndrome, we have characterized a mouse model with insertion of an expression cassette encoding a β-galactosidase neomycin resistance fusion protein (β-Geo) into intron 50 of *Kmt2d* (*Mll2*) on mouse chromosome 15. Inclusion of a splice acceptor sequence and a 3′ end cleavage and polyadenylation signal at the 5′ and 3′ ends of the β-Geo cassette, respectively, is predicted to generate a truncated KMT2D protein with peptide sequence corresponding to the first 50 exons of *Kmt2d* fused to β-Geo, but lacking the SET domain and therefore methyltransferase activity (Fig. 1B and fig. S1A). As predicted from this targeting event, quantitative real-time polymerase chain reaction (PCR) analysis of *Kmt2d* messenger RNA in *Kmt2d*$^{+/\beta Geo}$ mice demonstrated normal abundance of sequence corresponding to exon 20 but a 50% reduction for exon 52, when compared to *Kmt2d*$^{+/+}$ littermates (Fig. 1C). Expression of a KMT2D–β-galactosidase fusion protein in *Kmt2d*$^{+/\beta Geo}$ animals demonstrated transcription and translation of the targeted allele (fig. S1B). Furthermore, chromatin immunoprecipitation followed by next-generation sequencing (ChIP-seq) on splenic cells from *Kmt2d*$^{+/\beta Geo}$ mice and *Kmt2d*$^{+/+}$ littermates using an antibody against H3K4me3 revealed an overall genome-wide decrease in H3K4me3 in *Kmt2d*$^{+/\beta Geo}$ mice (Fig. 1D), supporting the predicted functional consequences of the mutant allele. Finally, *Kmt2d*$^{+/\beta Geo}$ mice demonstrated facial features that are consistent with Kabuki syndrome including flattened snout (fig. S2A) and downward rotation of the ear canal (fig. S2B). Blinded analysis of x-rays of *Kmt2d*$^{+/\beta Geo}$ mice revealed a significantly shorter maxilla ($P < 0.005$) when compared to *Kmt2d*$^{+/+}$ littermates (fig. S2, B and C), as judged by the extent of protrusion beyond the mandible (fig. S2C).

Kmt2d$^{+/\beta Geo}$ mice demonstrate hippocampal memory defects

Disruption of several histone-modifying enzyme genes has been shown to lead to hippocampal memory defects in mice, illustrating a critical role for epigenetic homeostasis in memory acquisition (9–11). *Kmt2d*$^{+/\beta Geo}$ mice showed significant deficits in novel object recognition ($P < 0.05$; Fig. 1E), Morris water maze probe trial ($P < 0.005$; Fig. 1F), and contextual fear conditioning ($P < 0.05$; fig. S3) when compared to *Kmt2d*$^{+/+}$ littermates, all consistent with hippocampal memory dysfunction. When performed before the hidden platform stage of training, the flag-training phase of the Morris water maze did not reveal significant differences between *Kmt2d*$^{+/\beta Geo}$ and *Kmt2d*$^{+/+}$ littermates (fig. S4). *Kmt2d*$^{+/\beta Geo}$ mice did not show decreased activity (fig. S5A), reduced grip strength (fig. S5B), or slower swim speeds (fig. S5C), any of which would be indicative of a more generalized limitation of performance potential in these assays. There were no significant differences in the time that it took *Kmt2d*$^{+/\beta Geo}$ mice to identify the platform (escape latency) compared to *Kmt2d*$^{+/+}$ mice during the training phase (fig. S6).

Decreased dentate gyrus volume and defective neurogenesis in *Kmt2d*$^{+/\beta Geo}$ mice

Immunofluorescence analyses revealed particularly high levels of expression of KMT2D protein in the dentate gyrus granule cell layer of the hippocampus in *Kmt2d*$^{+/+}$ mice (Fig. 2A) and a marked deficiency of H3K4me3 in the dentate gyrus granule cell layer of *Kmt2d*$^{+/\beta Geo}$ mice compared to *Kmt2d*$^{+/+}$ littermates ($P < 0.05$; Fig. 2, B and C). We also saw a similar deficiency of H3K4me3 in the pyramidal layer of the hippocampus ($P < 0.01$; fig. S7). The amount of H3K4me3 showed substantial cell-to-cell variability in *Kmt2d*$^{+/\beta Geo}$ animals (Fig. 2B), suggesting that variation in cell state or identity within the granule cell layer or dentate gyrus may influence vulnerability to the consequences of heterozygous *Kmt2d* disruption. *Kmt2d*$^{+/\beta Geo}$ mice showed a significant decrease in body weight but not brain weight ($P < 0.05$; fig. S8), and had reduced dentate gyrus granule cell layer volume when standardized to brain weight ($P < 0.05$; Fig. 2, D and E). This correlated with reduced neurogenesis in the granule cell layer of *Kmt2d*$^{+/\beta Geo}$ mice, as evidenced by significantly reduced expression of both doublecortin (DCX) (12) ($P < 0.001$; Fig. 2, F and G) and 5-ethynyl-2′deoxyuridine (EdU) staining, a marker of both neurogenesis in the granule cell layer and a marker of neuronal survival when monitored 30 days after labeling ($P < 0.01$; fig. S9). Confocal microscopy revealed an apparent decrease in dendritic branching complexity of DCX-positive (DCX$^+$) cells in the granule cell layer of *Kmt2d*$^{+/\beta Geo}$ mice (fig. S10). However, given the decreased amounts of DCX$^+$cells in these mice, further work is needed to determine whether this is a true or primary manifestation of *Kmt2d* deficiency. Staining with an antibody against activated caspase 3 did not reveal evidence for enhanced cell death in the dentate gyrus in heterozygous-targeted animals (fig. S11). To explore whether there are hippocampal memory defects in patients with Kabuki syndrome, we analyzed comprehensive neuropsychological testing performed on three patients with known disease-causing mutations in *KMT2D* (Table 1). Although not all deficiencies observed can be explained by hippocampal dysfunction, patients consistently had abnormalities in tasks known to be associated with dentate gyrus function (13–15). Other functions linked to other regions of the hippocampus (16) were also abnormal in some patients, as were some tasks not linked to hippocampus, indicating that other cell populations in the central nervous

system may also play a role. These data support the hypothesis that observations in *Kmt2d*$^{+/\beta Geo}$ mice are, at least in part, reminiscent of findings in Kabuki syndrome in human patients.

Reporter alleles for epigenetic modifications in embryonic fibroblasts from *Kmt2d*$^{+/\beta Geo}$ mice

We created epigenetic reporter systems that monitored either H4 acetylation or H3K4 trimethylation machinery activity in an effort to determine whether there was an ongoing activity deficiency in cells from *Kmt2d*$^{+/\beta Geo}$ mice (Fig. 3A). Both reporter alleles encode halves of green fluorescent protein (GFP) separated by a flexible linker region (17) with a histone tail and a histone reader at the N and C termini, respectively. When the histone tail corresponding to either H4 or H3 is modified by acetylation or methylation, respectively, GFP structure and function are reconstituted, as detected by a fluorescent readout (Fig. 3B). The acetyl reporter protein quantifies the activity of the acetylation machinery (acetylation of H4 specifically at sites K5, K8, K12, and K16) and comprises an H4 tail (residues 1 to 30) on one end and a TATA box–binding protein (TBP)–associated factor II (TAFII) bromodomain on the other end (Fig. 3A). The TAFII bromodomain only recognizes and binds to the acetylated H4 tail. This acetylation-dependent reporter protein demonstrated a linear fluorescence response when quantified by fluorescence-activated cell sorting (FACS) in the presence of increasing amounts of suberoylanilide hydroxamic acid (SAHA), an HDACi, in culture systems (Fig. 3, C and D). Saturation of this response correlated well with immunoblot data using antibodies to the modified H4 tail (18). This response was attenuated by cotransfection with a construct encoding an HDAC (fig. S12) and absent upon mutagenesis of all potential acetylation sites (Fig. 3E), attesting to its specificity. The H3K4 trimethylation reporter allele encodes the H3 tail (residues 1 to 40) on one end and the TBP-associated factor III (TAF3) plant homeodomain (PHD) on the other end, which binds to trimethylated K4 on H3 (Fig. 3A). The H3K4 trimethylation reporter also demonstrated a dose response with increasing amounts of the HDACi AR-42 (Fig. 3F), in keeping with previous work suggesting that AR-42 can also influence the methylation status of H3K4 through inhibition of demethylases (19). Activity was greatly attenuated upon mutagenesis of critical residues (M882A, D890A/W891A) (20, 21) in the TAF3 reader domain (Fig. 3G) or with mutation of K4 (H3K4Q) in the H3 tail (Fig. 3G). Both reporter alleles showed decreased activity when stably introduced into embryonic fibroblasts derived from *Kmt2d*$^{+/\beta Geo}$ mice when compared to *Kmt2d*$^{+/+}$ littermates (fig. S13). H3K4 trimethylation activity was enhanced upon treatment of *Kmt2d*$^{+/\beta Geo}$ cells with HDAC inhibitors AR-42 or MS275 (Fig. 3H and fig. S14A). An analysis of transfection efficacy in cells with both genotypes indicated comparable transfection efficacy (fig. S14B).

Rescue of neurogenesis and H3K4 trimethylation deficiencies in *Kmt2d*$^{+/\beta Geo}$ mice treated with the HDACi AR-42

Because of the ability of HDACi to increase H3K4 trimethylation in vitro in *Kmt2d*$^{+/\beta Geo}$ cells, we next asked whether the H3K4 trimethylation deficiency seen in the dentate gyrus granule cell layer of *Kmt2d*$^{+/\beta Geo}$ mice could be attenuated or reversed upon in vivo postnatal treatment with an HDACi. Previously, the HDAC inhibitors AR-42 and MS275 have both been shown to increase H3K4 trimethylation and histone acetylation (19). AR-42

appeared to have the strongest effect on H3K4me3 (19) and was shown to be well tolerated in mice in a long-term preclinical trial (22); it was therefore chosen for in vivo studies. We started at an AR-42 dose of 25 mg/kg per day, previously used in mouse models of prostate cancer (19), commencing at 20 weeks of age and continuing for 2 weeks. This dose increased H3K4 trimethylation in the granule cell layer in *Kmt2d*$^{+/\beta Geo}$ mice, compared to untreated mutant littermates (fig. S15, A and B), to a level that was indistinguishable from treated *Kmt2d*$^{+/+}$ animals. Unexpectedly, however, this dose of AR-42 was associated with decreased DCX expression in the granule cell layer in both young (1- to 2-month-old) and old (5- to 6-month-old) *Kmt2d*$^{+/+}$ and *Kmt2d*$^{+/\beta Geo}$ mice (fig. S15, C and D). Given the known cytotoxic potential of AR-42 (19, 23), we next tested doses of 5 and 10 mg/kg per day, and observed a dose-dependent increase in H3K4me3 and preservation or restoration of DCX expression in *Kmt2d*$^{+/+}$ or *Kmt2d*$^{+/\beta Geo}$ animals in both age groups, respectively (Fig. 4, A to D, and fig. S15D). This dose also led to a genome-wide increase in H3K4me3 in spleen cells from *Kmt2d*$^{+/\beta Geo}$ mice when compared to *Kmt2d*$^{+/+}$ littermates on vehicle (Fig. 4E) in association with normalization of expression of *Klf10* (fig. S16), a known KMT2D target gene (24). This dose appeared to overcorrect the deficiency (Fig. 4E), which could be observed when representing data as MA plots (the relationship between log ratios and mean averages, fig. S17) or visualizing the shifts in balance among the two states (fig. S18). We also compared other state combinations with the same representations, showing a relative normalization of genome-wide H3K4me3 in *Kmt2d*$^{+/\beta Geo}$ mice treated with AR-42 when compared to *Kmt2d*$^{+/+}$ littermates that did (fig. S17E) or did not (fig. S17B) receive drug. The bigger effect at lower intensity $\log_2$ counts per million fits with data from ablation of the Rubinstein-Taybi gene encoding CREB (cyclic adenosine 3′,5′-monophosphate response element–binding protein)–binding protein (CBP), which has dose-dependent effects on gene expression thought to depend on the strength of recruitment for a particular site (25).

Improvement of hippocampal memory defects in *Kmt2d*$^{+/\beta Geo}$ mice treated with AR-42

In keeping with the hypothesis that abnormal granule cell layer neurogenesis contributes to functional deficits, we found that performance in hippocampal memory testing correlated with AR-42 dose-dependent effects on DCX expression. Specifically, both *Kmt2d*$^{+/+}$ and *Kmt2d*$^{+/\beta Geo}$ mice showed improved performance on Morris water maze platform crossing during probe trial (26) in response to AR-42 (10 mg/kg per day) ($P < 0.001$), with a greater response in *Kmt2d*$^{+/\beta Geo}$ animals and no significant difference between genotypes in the treatment group ($P = 0.27$; Fig. 4F).

DISCUSSION

Previous studies have associated structural abnormalities of the dentate gyrus with impaired neurogenesis and hippocampal memory defects (27, 28). In accordance with the previously observed phenotype in *Kmt2b*-targeted mice (7), we found that heterozygosity for a loss-of-function *Kmt2d* allele associates a deficiency of H3K4me3 in the dentate gyrus granule cell layer with hippocampal memory defects in a mouse model of Kabuki syndrome. Support for a causal relationship is now increased by our observation that memory deficits in a mouse

model of Kabuki syndrome can be prevented or even reversed through systemic delivery of drugs that directly influence the histone modification events that favor chromatin opening.

Our data support the hypothesis that the neurodevelopmental deficiency in Kabuki syndrome is maintained by an impairment of adult neurogenesis because of an imbalance between open and closed chromatin states for critical target genes. In this light, other Mendelian disorders involving the histone modification machinery, now numbering more than 40 (29), might be amenable to therapeutic intervention with HDAC inhibitors (30–32). In keeping with this concept, neurological phenotypes in mouse models of Rubinstein-Taybi syndrome with haploinsufficiency for the gene encoding the histone acetyltransferase *Cbp* respond to intracerebroventricular or intraperitoneal administration of the HDACi SAHA or trichostatin A, respectively (33, 34); however, no cellular mechanism was described. The specific correlation between H3K4me3 and neurogenesis within the dentate gyrus of Kabuki syndrome mice offers a potential unifying mechanism for hippocampal memory defects seen in inherited defects of the histone modification machinery (10, 11, 33, 34). The further positive correlation of these events with functional outcome supports the hypothesis that the fate of the granule cell layer in the dentate gyrus is a critical determinant of both disease pathogenesis and treatment. More work is needed to determine the relative contribution of precursor cell recruitment, differentiation, proliferation, and survival (35, 36). Future studies using lineage-specific *Kmt2d* targeting will help to elucidate the contribution of individual cell populations (granule cell layer, pyramidal layer, and molecular layer of the cerebellum) to specific neurodevelopmental phenotypes.

Although there is an overall decrease in H3K4me3 in the dentate gyrus granule cell layer of $Kmt2d^{+/\beta Geo}$ mice, we note substantial cell-to-cell variation. This might reflect redundancy of enzymes capable of adding the H3K4 trimethylation mark (7) that could vary in their expression (and therefore compensation capacity) in a cell type–dependent (for example, differentiation state) or cell state–dependent (for example, electrochemical environment) manner. Alternatively, this could indicate that stochastic events thought to contribute to epigenetic individuality (37) play a role.

There is precedent that HDACi increases not only histone acetylation but also H3K4 trimethylation (19). Our indicators nicely illustrate coupling between H4 acetylation and H3K4 trimethylation, with $Kmt2d^{+/\beta Geo}$ mice having defects in both systems. Although AR-42 was used here for this proof of principle study, such a generalized HDACi may have an unacceptable toxicity profile in patients. The reporter alleles described here have the potential for application in small-molecule screens to identify drugs with greater potency, specificity, and tolerance. There are also many U.S. Food and Drug Administration–approved medications, some that have had longstanding clinical use, that influence epigenetic modifications in addition to their originally established functions. An example is the anti-epileptic agent valproic acid, which was recently shown to be a potent HDACi (38). Several widely used supplements or dietary substances, such as folic acid, genistein, and curcumin, are known to influence epigenetic modifications (39). A recent publication suggests that ketosis, as achieved in a ketogenic diet, might favor chromatin opening through β-hydroxybutyrate, an endogenous HDACi (40). This indicates the potential that dietary manipulations, such as a ketogenic diet, might have another therapeutic avenue for

treatment in disorders with a deficiency of open chromatin, such as Kabuki syndrome. These observations may inform the question of potential toxicity of interventions that have broad effects on pervasive epigenetic events. The apparent tolerance to chronic use of such agents during postnatal life likely reflects, at least in part, the complex context within which gene transcription and ultimate function are achieved. Contributing factors include DNA modifications, a repertoire of both positive and negative effectors of transcription, and feedback mechanisms that titrate both gene expression and protein function. In this light, the predominant influence of agents such as HDACi as therapies may prove permissive for correction of pathologic alterations in physiologic gene expression and function rather than obligate and therefore less conducive to homeostasis.

Although we were able to demonstrate a beneficial effect of AR-42 treatment on neurogenesis at two different ages (1 to 2 months and 5 to 6 months), suggesting that this subphenotype of Kabuki syndrome may be treatable even in adulthood, it is well established that neurogenesis potential is age-restricted (41). It will be essential to further refine the window of opportunity to influence neurogenesis in the granule cell layer in both mouse models and patients. Although our data suggest that neurogenesis and hippocampal memory can be recovered after 2 weeks of treatment with AR-42, it is unclear if this response can be sustained even in the presence of chronic treatment. It is also possible, but as yet unproven, that brief treatment in early postnatal stages will result in the expansion of a stable population of cells within the granule cell layer (despite an ongoing relative deficiency of methyltransferase function) and hence achieve long-term recovery of neurologic function. Finally, our ChIP-seq experiments suggest that AR-42 at a dose of 10 mg/kg per day led to the most improvement in functional studies (Fig. 4D) but overcorrection of genome-wide H3K4me3 (Fig. 4E). Given the favorable tolerance profile of high-dose HDACi when used for cancer treatment, this may not be a limiting factor. However, new challenges may arise when HDACis are used chronically for Kabuki syndrome or other neurodevelopmental disorders. The combination of in vivo ChIP-seq analyses and in vitro reporter allele performance with regard to H3K4me3 status may ultimately allow optimization in the selection of agent and dose for therapeutic purposes.

Potential limitations of this study include the use of a single heterozygous *Kmt2d* targeted allele that introduces a β-Geo expression cassette into the open reading frame. Although this strategy should recapitulate haploinsufficiency for KMT2D, as seen in Kabuki syndrome patients heterozygous for nonsense alleles, a gain-of-function contribution of the fusion protein cannot be formally excluded. There are also inherent limitations in the use of mouse models in the study of human neurocognitive disorders. Finally, lineage-specific cell targeting will be required to mechanistically validate the correlative link between performance deficits and defects in adult neurogenesis in the dentate gyrus.

In conclusion, our work suggests that a postnatally ongoing and reversible deficiency of granule cell layer H3K4me3, in association with alterations in adult neurogenesis, underlies intellectual disability in a mouse model of Kabuki syndrome. This work adds to the emerging view that multiple genetic etiologies of intellectual disability may be amenable to postnatal therapies (42–44).

MATERIALS AND METHODS

Study design

The purposes of this study were to explore the pathophysiological sequence in Kabuki syndrome, a Mendelian disorder of the epigenetic machinery, and to seek robust disease-associated phenotypes, which could be used to monitor therapeutic response. We hypothesized that because both causes of Kabuki syndrome involve the transition from closed to open chromatin, this disorder might be caused by a general imbalance between open and closed chromatin states (favoring closed chromatin) and this ongoing deficiency might be ameliorated with agents that favor chromatin opening such as HDACi. At least 3 to 4 biological replicates were used for each biochemical analysis, whereas a sample size of at least 8 to 10 per group was used for behavioral testing. Data collection occurred for a predetermined period of time, as dictated by literature- or core facility–based standards, and no exclusion criteria were applied. All analyses were performed by examiners blinded to genotype and/or treatment arm. For drug treatments, animals were randomly assigned to treatment arms with approximately equivalent numbers in each group. Box and whisker plots identify RStudio-defined outliers (shown as circles), but all data points were used in statistical analyses.

Epigenetic reporter alleles

Epigenetic reporter alleles were synthesized (OriGene) using published sequences for component elements (17, 45). Single-nucleotide mutations were created using the QuikChange Lightening kit (Agilent Technologies Inc.). For H4ac indicator, we introduced K5R, K8R, K12R, K16R, and K20R (MUT indicator). For H3K4me3 indicator, we introduced K4Q and D890A/W891A and M882A (three separate constructs). For transient transfections, mouse embryonic fibroblasts (see below) were transfected with FuGENE HD (Promega) 48 hours before FACS. Transfection efficiency of reporter alleles was comparable in transiently transfected MEFs derived from mice of both genotypes ($Kmt2d^{+/\beta Geo}$ and $Kmt2d^{+/+}$), as measured by real-time PCR of genomic DNA. For drug stimulation, drug was added to the medium 24 hours before FACS. For stable transfections in T293 (American Type Culture Collection) cells, blasticidin (10 μg/ml) (Life Technologies) was added to the medium for several weeks. For stable transfection in MEFs, the reporter was transferred to a ViraPower Lentiviral Expression System (Life Technologies). After selection with blasticidin, the drug of interest was added 24 hours before FACS. SAHA, AR-42, and MS275 were purchased from Selleck Chemicals. FACS was performed using either a FACSCalibur (BD Biosciences) or a FACSVerse (BD Biosciences) system with comparable results. FACS data were analyzed using FlowJo (Tree Star Inc.). A plasmid expressing HDAC3 was acquired from Addgene (plasmid 13819) and transfected into a stable cell line carrying the H4 acetyl reporter allele.

Animals

Our mouse model, $Kmt2d^{+/\beta Geo}$, also named $Mll2Gt^{(RRt024)Byg}$, was acquired from Bay Genomics (University of California). All experimental mice were on a mixed C57BL/6J and 129/SvEv background. Expected Mendelian ratios were observed when heterozygous animals were bred to wild type. In heterozygous crosses, however, there was uniform

embryonic lethality of homozygotes by ED12, the earliest developmental stage assayed. For treatment with AR-42, mice were orally gavaged daily with drug (Selleck Chemicals) solubilized in vehicle (0.5% methylcellulose, 0.1% Tween-80, water) or with vehicle alone. Drug delivery information was provided by C.S. Chen and S.K. Kulp from Ohio State University (19). Drug was administered for 14 days, and mice were sacrificed on day 15. Morris water maze testing was initiated at day 7, and a dose of 10 mg/kg per day was used for these studies. For quantification of DCX^+ cells, doses of 0, 5, 10, and 25 mg/kg per day were used. Genotyping was performed using primers B-GeoF-(CAAATGGCGAT-TACCGTTGA) and B-GeoR-(TGCCCAGTCATAGCCGAATA), which are specific for the targeted allele, and TcrdF-(CAAATGTTGC-TTGTCTGGTG) and TcrdR-(GTCAGTCGAGTGCACAGTTT), which control for sufficient DNA concentration. Real-time PCR using the same primers allows discrimination between the heterozygous and homozygous state for the targeted allele. Thymus was dissected from a wild-type neonatal mouse and flash-frozen in optimal cutting temperature (OCT). Slides were fixed with 4% paraformaldehyde for 30 min. All experiments were performed using mouse protocols approved by the Animal Care and Use Committee of Johns Hopkins University School of Medicine. The mouse protocols used for this study are in accordance with the guidelines used by the National Institutes of Health (NIH) for mouse care and handling.

Morris water maze testing

Mice were placed in a 1.1-m-diameter tank filled with room temperature water dyed with nontoxic white paint. For analysis purposes, the tank was divided into four quadrants, with one quadrant containing a small platform submerged 1.5 cm beneath the water. On each day of training, mice were placed in the tank in a random quadrant facing away from the center and were allowed to swim until they found the platform and were left there for 30 s. If they did not reach the platform after 60 s, they were placed on it for 30 s. Each mouse was given four trials per day (for 5 days) with no intertrial interval and subsequently returned to its home cage. Latency to reach the platform was measured during each trial. The day after the final day of training, the platform was removed for a probe trial where mice were placed in the tank for 90 s. The average number of crossings of the platform's previous location was recorded. Visible/flagged platform training was also performed for 3 days either before the hidden platform or after the probe trial, where a visible flag was placed on the submerged platform, and the time for each mouse to reach the platform was measured for each 60-s trial, four of which were run in the same way as the hidden platform training. For all training and probe testing, data were recorded both manually and electronically with ANY-maze software (San Diego Instruments) when applicable. Differences in the number of platform crossings during the probe trial were compared between groups with a Student's t test with significance value set at $P < 0.05$.

Retrospective analysis of neuropsychological testing on patients with Kabuki syndrome

A retrospective chart review was performed using data from patients that had clinically indicated neuropsychological testing at the Kennedy Krieger Institute (KKI) in years 2004 to 2014. We analyzed test results from the three individuals with most extensive testing available and a known disease-associated mutation in *KMT2D*. All patient data were collected after consenting patients and stored in secure electronic database at KKI. For this

particular analysis per Kennedy Krieger and Johns Hopkins organizational policy, additional Institutional Review Board review was not required (three or fewer patients). We divided the individual tasks into 16 categories and used literature to identify tasks known to be associated with dentate gyrus (13–15) or hippocampus (nondentate gyrus) (16).

ChIP-seq

Spleens were dissected from eight mice, four from each *kmt2d* genotype (+/βGeo or +/+), where half of each genotype was treated with AR-42 and half with vehicle only. Spleens were minced and passed through a 40-mm cell strainer to obtain single-cell suspensions. Ten million cells were used for each ChIP-seq experiment after the native chromatin immunoprecipitation protocol, as previously described (46), using a ChIP-grade antibody against H3K4me3 (9727, Cell Signaling Technology).

ChIP-seq data analysis

Sequencing was performed using a MiSeq system (Illumina). Paired-end 26–base pair reads (4.8 to 9.6 million) were obtained per sample (table S1). Reads were aligned to the *Mus musculus* genome, version mm10, using Bowtie 2 (47). We examined each sample with regard to alignment rate as well as FRIP (fraction of reads in peaks), a measure of the ChIP efficiency (table S1). FRIP was computed on the basis of peaks called only on specific samples using MACS version 1.4.2 (48). For analysis, reads were merged into one meta-sample and peak calling was performed using MACS version 1.4.2 (48). This allowed definition of a superset of 33,517 peaks in one or more samples. The number of reads overlapping a peak was computed using BEDTools version 2.17.0 (49) in the following way: each paired-end read was converted to a single interval containing both mate coordinates (effectively filling in the insert), and these intervals were examined for overlaps with the superset of peaks. This created a peak-by-sample matrix of read counts. Differential binding was assessed using the GLM functionality (50) in edgeR version 3.5.27 (51). A single model was fit, using all eight samples, with tag-wise variance estimation. Different contrasts were examined corresponding to the different hypotheses considered in the main text, and peaks were considered differentially bound if they had a Benjamini-Hochberg corrected *P* values less than 5%. Fold change and overall abundance were calculated as per edgeR.

Statistics and plots

For all box plots generated through RStudio (RStudio Inc.), the margins of the box show the upper and lower quartiles, the central line shows the median, and the whiskers show the range. Circles denote outliers as defined by the RStudio algorithm. For all column, line, and scatterplot graphs (generated through Microsoft Excel), the error bars represent SEM, with the data point representing the mean of each applicable group. Unless otherwise stated, significance between two groups was calculated with a Student's *t* test using a significance value of $P < 0.05$. Two-way repeated-measures analyses of variance (ANOVAs) were calculated with SPSS (IBM). For every calculated *P* value, the stated *n* represents the number of animals for each group contributing to that comparison. For *P* value nomenclature, $*P < 0.05$, $**P < 0.01$, $^{\dagger}P < 0.005$, $^{\dagger\dagger}P < 0.001$.

Supplementary Material

Refer to Web version on PubMed Central for supplementary material.

Acknowledgments

We would like to acknowledge M. Pletnikov, Director of The Behavioral Core at the School of Medicine, for recommendations regarding behavioral test selection and C. S. Chen and S. K. Kulp from the Ohio State University for information regarding drug preparation protocols. We would like to thank S. Fontana for advice on culturing MEFs, M. Swaim and E. Gallofor advice on FACS, and M. Zeledon for advice on EdU staining. We would like to thank K. Smith and A. Doyle for reading the manuscript.

Funding: This work was supported by grants to H.C.D. by the Smilow Center for Marfan Syndrome Research and the Howard Hughes Medical Institute and to H.T.B. by the NIH Director's Early Independence Award (DP5OD017877) and a Young Investigator Research Grant from the American Academy of Pediatrics Section on Genetics and Birth Defects.

REFERENCES AND NOTES

1. Ng SB, Bigham AW, Buckingham KJ, Hannibal MC, McMillin MJ, Gildersleeve HI, Beck AE, Tabor HK, Cooper GM, Mefford HC, Lee C, Turner EH, Smith JD, Rieder MJ, Yoshiura K, Matsumoto N, Ohta T, Niikawa N, Nickerson DA, Bamshad MJ, Shendure J. Exome sequencing identifies *MLL2* mutations as a cause of Kabuki syndrome. Nat. Genet. 2010; 42:790–793. [PubMed: 20711175]
2. Lederer D, Grisart B, Digilio MC, Benoit V, Crespin M, Ghariani SC, Maystadt I, Dallapiccola B, Verellen-Dumoulin C. Deletion of KDM6A, a histone demethylase interacting with MLL2, in three patients with Kabuki syndrome. Am. J. Hum. Genet. 2012; 90:119–124. [PubMed: 22197486]
3. Miyake N, Mizuno S, Okamoto N, Ohashi H, Shiina M, Ogata K, Tsurusaki Y, Nakashima M, Saitsu H, Niikawa N, Matsumoto N. KDM6A point mutations cause Kabuki syndrome. Hum. Mutat. 2013; 34:108–110. [PubMed: 23076834]
4. Brus M, Keller M, Lévy F. Temporal features of adult neurogenesis: Differences and similarities across mammalian species. Front. Neurosci. 2013; 7:135. [PubMed: 23935563]
5. Altman J. Are new neurons formed in the brains of adult mammals? Science. 1962; 135:1127–1128. [PubMed: 13860748]
6. Hunter S, Jones P, Mitchell A, Apweiler R, Attwood TK, Bateman A, Bernard T, Binns D, Bork P, Burge S, de Castro E, Coggill P, Corbett M, Das U, Daugherty L, Duquenne L, Finn RD, Fraser M, Gough J, Haft D, Hulo N, Kahn D, Kelly E, Letunic I, Lonsdale D, Lopez R, Madera M, Maslen J, McAnulla C, McDowall J, McMenamin C, Mi H, Mutowo-Muellenet P, Mulder N, Natale D, Orengo C, Pesseat S, Punta M, Quinn AF, Rivoire C, Sangrador-Vegas A, Selengut JD, Sigrist CJ, Scheremetjew M, Tate J, Thimmajanarthanan M, Thomas PD, Wu CH, Yeats C, Yong SY. InterPro in 2011: New developments in the family and domain prediction database. Nucleic Acids Res. 2012; 40:D306–D312. [PubMed: 22096229]
7. Kerimoglu C, Agis-Balboa RC, Kranz A, Stilling R, Bahari-Javan S, Benito-Garagorri E, Halder R, Burkhardt S, Stewart AF, Fischer A. Histone-methyltransferase MLL2 (KMT2B) is required for memory formation in mice. J. Neurosci. 2013; 33:3452–3464. [PubMed: 23426673]
8. Bögershausen N, Bruford E, Wollnik EB. Skirting the pitfalls: A clear-cut nomenclature for H3K4 methyltransferases. Clin. Genet. 2013; 83:212–214. [PubMed: 23130995]
9. Guan Z, Giustetto M, Lomvardas S, Kim JH, Miniaci MC, Schwartz JH, Thanos D, Kandel ER. Integration of long-term-memory-related synaptic plasticity involves bidirectional regulation of gene expression and chromatin structure. Cell. 2002; 111:483–493. [PubMed: 12437922]
10. Gupta S, Kim SY, Artis S, Molfese DL, Schumacher A, Sweatt JD, Paylor RE, Lubin FD. Histone methylation regulates memory formation. J. Neurosci. 2010; 30:3589–3599. [PubMed: 20219993]
11. Cohen-Armon M, Visochek L, Katzoff A, Levitan D, Susswein AJ, Klein R, Valbrun M, Schwartz JH. Long-term memory requires polyADP-ribosylation. Science. 2004; 304:1820–1822. [PubMed: 15205535]

12. Rao MS, Shetty AK. Efficacy of doublecortin as a marker to analyse the absolute number and dendritic growth of newly generated neurons in the adult dentate gyrus. Eur. J. Neurosci. 2004; 19:234–246. [PubMed: 14725617]
13. Kesner RP. An analysis of the dentate gyrus function. Behav. Brain Res. 2013; 254:1–7. [PubMed: 23348108]
14. Morris AM, Churchwell JC, Kesner RP, Gilbert PE. Selective lesions of the dentate gyrus produce disruptions in place learning for adjacent spatial locations. Neurobiol. Learn. Mem. 2012; 97:326–331. [PubMed: 22390856]
15. Epp JR, Haack AK, Galea LA. Activation and survival of immature neurons in the dentate gyrus with spatial memory is dependent on time of exposure to spatial learning and age of cells at examination. Neurobiol. Learn. Mem. 2011; 95:316–325. [PubMed: 21216298]
16. Brickman AM, Stern Y, Small SA. Hippocampal subregions differentially associate with standardized memory tests. Hippocampus. 2011; 21:923–928. [PubMed: 20824727]
17. Baird GS, Zacharias DA, Tsien RY. Circular permutation and receptor insertion within green fluorescent proteins. Proc. Natl. Acad. Sci. U.S.A. 1999; 96:11241–11246. [PubMed: 10500161]
18. Munshi A, Tanaka T, Hobbs ML, Tucker SL, Richon VM, Meyn RE. Vorinostat, a histone deacetylase inhibitor, enhances the response of human tumor cells to ionizing radiation through prolongation of γ-H2AX foci. Mol. Cancer Ther. 2006; 5:1967–1974. [PubMed: 16928817]
19. Huang PH, Chen CH, Chou CC, Sargeant AM, Kulp SK, Teng CM, Byrd JC, Chen CS. Histone deacetylase inhibitors stimulate histone H3 lysine 4 methylation in part via transcriptional repression of histone H3 lysine 4 demethylases. Mol. Pharmacol. 2011; 79:197–206. [PubMed: 20959362]
20. Vermeulen M, Mulder KW, Denissov S, Pijnappel VW, van Schaik FM, Varier RA, Baltissen MP, Stunnenberg HG, Mann M, Timmers HT. Selective anchoring of TFIID to nucleosomes by trimethylation of histone H3 lysine 4. Cell. 2007; 131:58–69. [PubMed: 17884155]
21. van Ingen H, van Schaik FM, Wienk H, Ballering J, Rehmann H, Dechesne AC, Kruijzer JA, Liskamp RM, Timmers HT, Boelens R. Structural insight into the recognition of the H3K4me3 mark by the TFIID subunit TAF3. Structure. 2008; 16:1245–1256. [PubMed: 18682226]
22. Jacob A, Oblinger J, Bush ML, Brendel V, Santarelli G, Chaudhury AR, Kulp S, La Perle KM, Chen CS, Chang LS, Welling DB. Preclinical validation of AR42, a novel histone deacetylase inhibitor, as treatment for vestibular schwannomas. Laryngoscope. 2012; 122:174–189. [PubMed: 22109824]
23. Zhang S, Suvannasankha A, Crean CD, White VL, Chen CS, Farag SS. The novel histone deacetylase inhibitor, AR-42, inhibits gp130/Stat3 pathway and induces apoptosis and cell cycle arrest in multiple myeloma cells. Int. J. Cancer. 2011; 129:204–213. [PubMed: 20824695]
24. Guo C, Chang CC, Wortham M, Chen LH, Kernagis DN, Qin X, Cho YW, Chi JT, Grant GA, McLendon RE, Yan H, Ge K, Papadopoulos N, Bigner DD, He Y. Global identification of MLL2-targeted loci reveals MLL2's role in diverse signaling pathways. Proc. Natl. Acad. Sci. U.S.A. 2012; 109:17603–17608. [PubMed: 23045699]
25. Kasper LH, Lerach S, Wang J, Wu S, Jeevan T, Brindle PK. CBP/p300 double null cells reveal effect of coactivator level and diversity on CREB transactivation. EMBO J. 2010; 29:3660–3672. [PubMed: 20859256]
26. Garthe A, Kempermann G. An old test for new neurons: Refining the Morris water maze to study the functional relevance of adult hippocampal neurogenesis. Front. Neurosci. 2013; 7:63. [PubMed: 23653589]
27. Ansorg A, Witte OW, Urbach A. Age-dependent kinetics of dentate gyrus neurogenesis in the absence of cyclin D2. BMC Neurosci. 2012; 13:46. [PubMed: 22564330]
28. Denis-Donini S, Dellarole A, Crociara P, Francese MT, Bortolotto V, Quadrato G, Canonico PL, Orsetti M, Ghi P, Memo M, Bonini SA, Ferrari-Toninelli G, Grilli M. Impaired adult neurogenesis associated with short-term memory defects in NF-κB p50-deficient mice. J. Neurosci. 2008; 28:3911–3919. [PubMed: 18400889]
29. Berdasco M, Esteller M. Genetic syndromes caused by mutations in epigenetic genes. Hum. Genet. 2013; 132:359–383. [PubMed: 23370504]

30. Dash PK, Orsi SA, Moore AN. Histone deactylase inhibition combined with behavioral therapy enhances learning and memory following traumatic brain injury. Neuroscience. 2009; 163:1–8. [PubMed: 19531374]

31. Vecsey CG, Hawk JD, Lattal KM, Stein JM, Fabian SA, Attner MA, Cabrera SM, McDonough CB, Brindle PK, Abel T, Wood MA. Histone deacetylase inhibitors enhance memory and synaptic plasticity via CREB:CBP-dependent transcriptional activation. J. Neurosci. 2007; 27:6128–6140. [PubMed: 17553985]

32. Gräff J, Tsai LH. The potential of HDAC inhibitors as cognitive enhancers. Annu. Rev. Pharmacol. Toxicol. 2013; 53:311–330. [PubMed: 23294310]

33. Korzus E, Rosenfeld MG, Mayford M. CBP histone acetyltransferase activity is a critical component of memory consolidation. Neuron. 2004; 42:961–972. [PubMed: 15207240]

34. Alarcón JM, Malleret G, Touzani K, Vronskaya S, Ishii S, Kandel ER, Barco A. Chromatin acetylation memory and LTP are impaired in $CBP^{+/-}$ mice: A model for the cognitive deficit in Rubinstein-Taybi syndrome and its amelioration. Neuron. 2004; 42:947–959. [PubMed: 15207239]

35. Yang P, Guo L, Duan ZJ, Tepper CG, Xue L, Chen X, Kung HJ, Gao AC, Zou JX, Chen HW. Histone methyltransferase NSD2/MMSET mediates constitutive NF-κB signaling for cancer cell proliferation, survival, and tumor growth via a feed-forward loop. Mol. Cell. Biol. 2012; 32:3121–3131. [PubMed: 22645312]

36. Lubitz S, Glaser S, Schaft J, Stewart AF, Anastassiadis K. Increased apoptosis and skewed differentiation in mouse embryonic stem cells lacking the histone methyltransferase Mll2. Mol. Biol. Cell. 2007; 18:2356–2366. [PubMed: 17429066]

37. Bjornsson HT, Fallin MD, Feinberg AP. An integrated epigenetic and genetic approach to common human disease. Trends Genet. 2004; 20:350–358. [PubMed: 15262407]

38. Phiel CJ, Zhang F, Huang EY, Guenther MG, Lazar MA, Klein PS. Histone deacetylase is a direct target of valproic acid, a potent anticonvulsant, mood stabilizer, and teratogen. J. Biol. Chem. 2001; 276:36734–36741. [PubMed: 11473107]

39. Meeran SM, Ahmed A, Tollefsbol TO. Epigenetic targets of bioactive dietary components for cancer prevention and therapy. Clin. Epigenetics. 2010; 1:101–116. [PubMed: 21258631]

40. Shimazu T, Hirschey MD, Newman J, He W, Shirakawa K, Le Moan N, Grueter CA, Lim H, Saunders LR, Stevens RD, Newgard CB, Farese RV Jr, de Cabo R, Ulrich S, Akassoglou K, Verdin E, Suppression of oxidative stress by β-hydroxybutyrate. an endogenous histone deacetylase inhibitor. Science. 2013; 339:211–214. [PubMed: 23223453]

41. Martinez-Canabal A, Akers KG, Josselyn SA, Frankland PW. Age-dependent effects of hippocampal neurogenesis suppression on spatial learning. Hippocampus. 2013; 23:66–74. [PubMed: 22826108]

42. Guy J, Gan J, Selfridge J, Cobb S, Bird A. Reversal of neurological defects in a mouse model of Rett syndrome. Science. 2007; 315:1143–1147. [PubMed: 17289941]

43. Das I, Park JM, Shin JH, Jeon SK, Lorenzi H, Linden DJ, Worley PF, Reeves RH. Hedgehog agonist therapy corrects structural and cognitive deficits in a Down syndrome mouse model. Sci. Transl. Med. 2013; 5 201ra120.

44. Henderson C, Wijetunge L, Kinoshita MN, Shumway M, Hammond RS, Postma FR, Brynczka C, Rush R, Thomas A, Paylor R, Warren ST, Vanderklish PW, Kind PC, Carpenter RL, Bear MF, Healy AM. Reversal of disease-related pathologies in the fragile X mouse model by selective activation of GABAB receptors with arbaclofen. Sci. Transl. Med. 2012; 4 152ra128.

45. Souslova EA, Belousov VV, Lock JG, Strömblad S, Kasparov S, Bolshakov AP, Pinelis VG, Labas YA, Lukyanov S, Mayr LM, Chudakov DM. Single fluorescent protein-based Ca^{2+} sensors with increased dynamic range. BMC Biotechnol. 2007; 7:37. [PubMed: 17603870]

46. Gilfillan GD, Hughes T, Sheng Y, Hjorthaug HS, Straub T, Gervin K, Harris JR, Undlien DE, Lyle R. Limitations and possibilities of low cell number ChIP-seq. BMC Genomics. 2012; 13:645. [PubMed: 23171294]

47. Langmead B, Salzberg SL. Fast gapped-read alignment with Bowtie 2. Nat. Methods. 2012; 9:357–359. [PubMed: 22388286]

48. Zhang Y, Liu T, Meyer CA, Eeckhoute J, Johnson DS, Bernstein BE, Nusbaum C, Myers RM, Brown M, Li W, Liu XS. Model-based analysis of ChIP-Seq (MACS). Genome Biol. 2008; 9:R137. [PubMed: 18798982]

49. Quinlan AR, Hall IM. BEDTools: A flexible suite of utilities for comparing genomic features. Bioinformatics. 2010; 26:841–842. [PubMed: 20110278]

50. McCarthy DJ, Chen Y, Smyth GK. Differential expression analysis of multifactor RNA-Seq experiments with respect to biological variation. Nucleic Acids Res. 2012; 40:4288–4297. [PubMed: 22287627]

51. Robinson MD, McCarthy DJ, Smyth GK. edgeR: A Bioconductor package for differential expression analysis of digital gene expression data. Bioinformatics. 2010; 26:139–140. [PubMed: 19910308]

52. Loeys BL, Gerber EE, Riegert-Johnson D, Iqbal S, Whiteman P, McConnell V, Chillakuri CR, Macaya D, Coucke PJ, De Paepe A, Judge DP, Wigley F, C Davis E, Mardon HJ, Handford P, Keene DR, Sakai LY, Dietz HC. Mutations in fibrillin-1 cause congenital scleroderma: Stiff skin syndrome. Sci. Transl. Med. 2010; 23 23ra20.

53. Adamczyk A, Mejias R, Takamiya K, Yocum J, Krasnova IN, Calderon J, Cadet JL, Huganir RL, Pletnikov MV, Wang T. GluA3-deficiency in mice is associated with increased social and aggressive behavior and elevated dopamine in striatum. Behav. Brain Res. 2012; 229:265–272. [PubMed: 22285418]

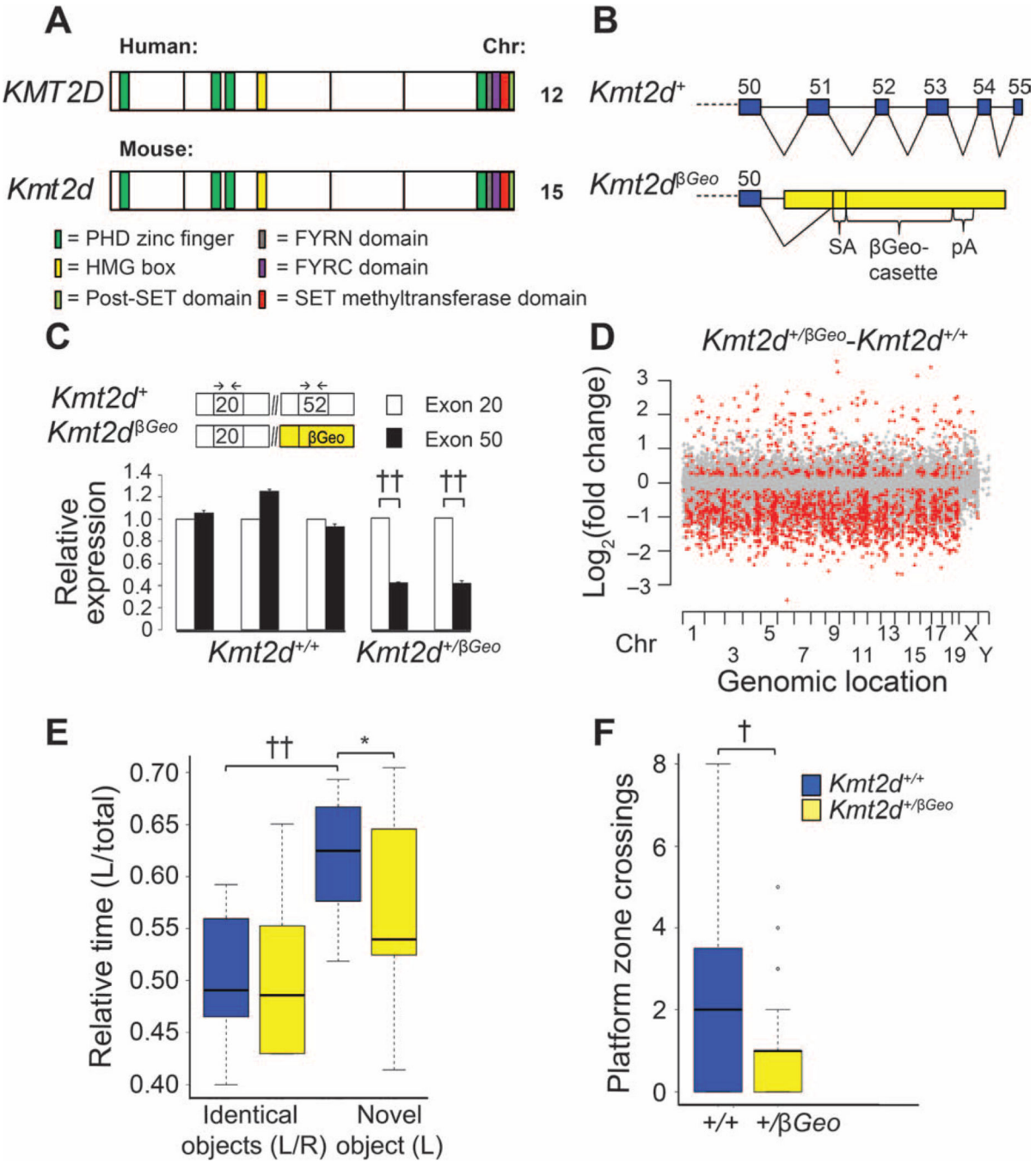

Fig. 1. Hippocampal memory defects in a *Kmt2d*$^{+/\beta Geo}$ mouse model of Kabuki syndrome

(**A**) Domain organization of *KMT2D* in human and mouse, with the relative position of the H3K4 methyltransferase SET domain indicated in red and other domains by additional colors. The human and murine chromosomal assignment (Chr) is shown. (**B**) The *Kmt2d*$^{\beta Geo}$ targeting event introduced a β-Geo cassette including a strong splice acceptor (SA) sequence and a 3′ cleavage and polyadenylation signal (pA) into intron 50 of *Kmt2d* on mouse chromosome 15 (fig. S1A). (**C**) Real-time PCR using primers specific for exons 20 or 52 of *Kmt2d* (arrows) confirmed a substantial reduction (~50%) in mRNA corresponding to

sequences distal to the β-Geo insertion site when compared to proximal sequences in *Kmt2d*$^{+/\beta Geo}$ mice, in comparison to *Kmt2d*$^{+/+}$ littermates. Results reflected three technical replicates for each of three *Kmt2d*$^{+/+}$ and two *Kmt2d*$^{+/\beta Geo}$ mice. (**D**) ChIP-seq revealed a genome-wide deficiency of H3K4me3 in cells from *Kmt2d*$^{+/\beta Geo}$mice when compared to cells from *Kmt2d*$^{+/+}$ littermates. A positive value indicates a higher locus-specific peak in *Kmt2d*$^{+/\beta Geo}$ mice. Each point corresponds to a genomic location with a peak in at least one sample. Significantly differentially bound loci are red, whereas others are gray. (**E**) There was no difference in positional preference between genotypes during the habituation phase [identical objects (L/R)] of the novel object recognition test. *Kmt2d*$^{+/\beta Geo}$ mice spent less time with a novel object (L) and more with a habituated object (R) compared to *Kmt2d*$^{+/+}$ littermates. *Kmt2d*$^{+/+}$ littermates also demonstrated significant improvement from habituation phase [novel object (L)], whereas *Kmt2d*$^{+/\beta Geo}$ mice did not. $n = 13$ (+/+), $n = 10$ (+/βGeo). (F) *Kmt2d*$^{+/\beta Geo}$ mice showed a reduced frequency in platform zone crossings during the probe trial phase of Morris water maze testing. $n = 48$ (+/+), $n = 32$ (+/βGeo). $^{*}P < 0.05$; $^{\dagger}P < 0.005$; $^{\dagger\dagger}P < 0.001$, *t* test.

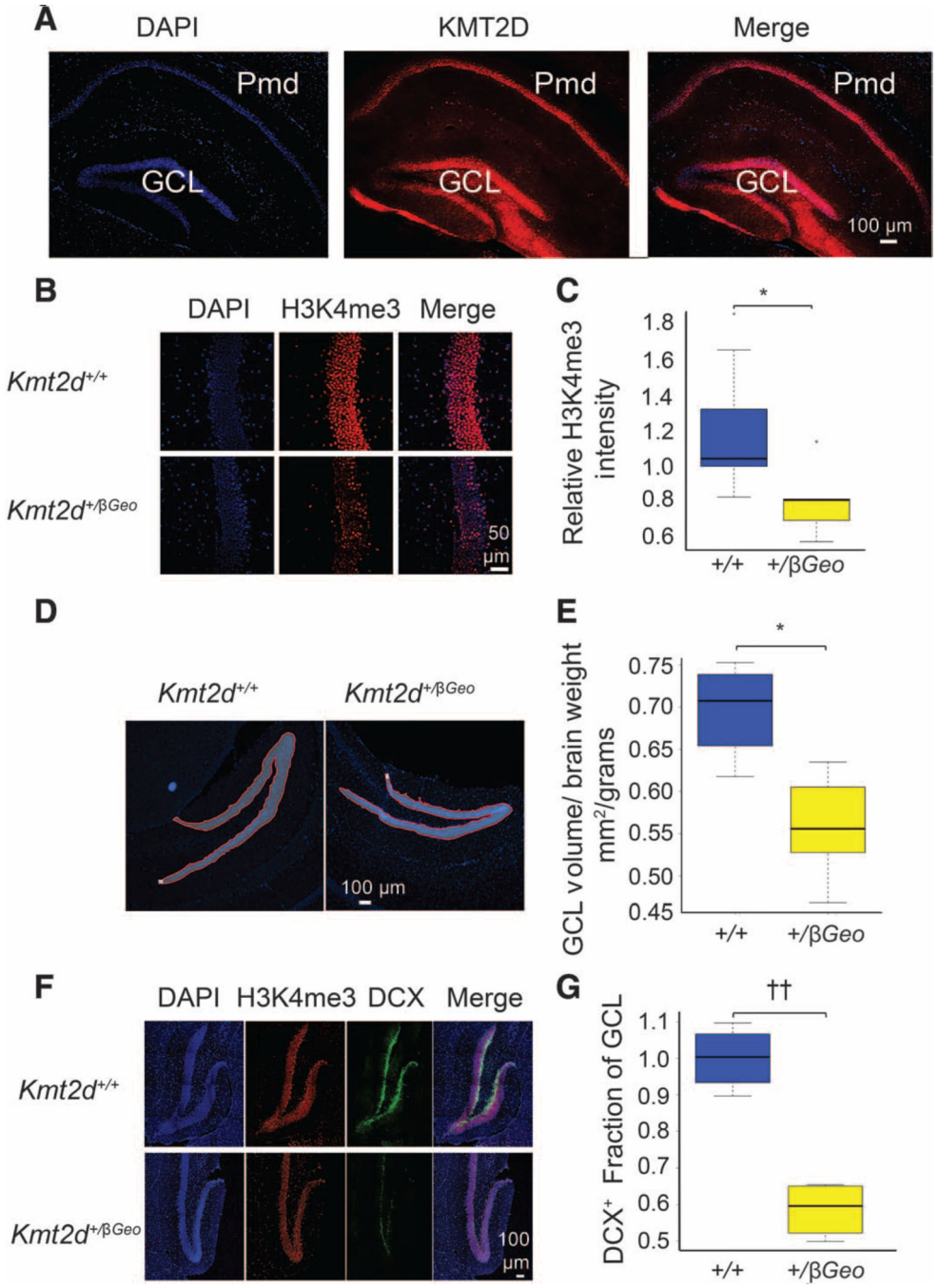

Fig. 2. A global deficiency of H3K4me3in the dentate gyrus associated with reduced granule cell layer volume and neurogenesis in *Kmt2d*$^{+/\beta Geo}$ mice

(**A**) Immunofluorescence revealed intense expression of KMT2D (red signal) in the dentate gyrus granule cell and pyramidal layers of *Kmt2d*$^{+/+}$ mice. (**B**) Immunofluorescence for H3K4me3 (red) and 4′,6-diamidino-2-phenylindole (DAPI) (blue) in the granule cell layer of *Kmt2d*$^{+/\beta Geo}$ mice and *Kmt2d*$^{+/+}$littermates. (**C**) Quantification revealed a reduced H3K4me3/DAPI signal intensity ratio within the granule cell layer of *Kmt2d*$^{+/\beta Geo}$ mice compared to *Kmt2d*$^{+/+}$ littermates. *n* = 9 (+/+), *n* = 5 (+/βGeo). (**D** and **E**) Calculation of

granule cell layer area (red outline) in every sixth brain slice allowed the demonstration of reduced granule cell layer volume in *Kmt2d*$^{+/\beta Geo}$ mice compared to *Kmt2d*$^{+/+}$ littermates. $n = 4$ (+/+), $n = 5$ (+/βGeo). (**F** and **G**) Immunofluorescence revealed reduced representation of cells positive for DCX, a marker for neurogenesis, in the granule cell layer of *Kmt2d*$^{+/\beta Geo}$ mice compared to *Kmt2d*$^{+/+}$ littermates. $n = 4$ (+/+), $n = 4$ (+/βGeo). $^{*}P < 0.05$; $^{\dagger\dagger}P < 0.001$, *t* test.

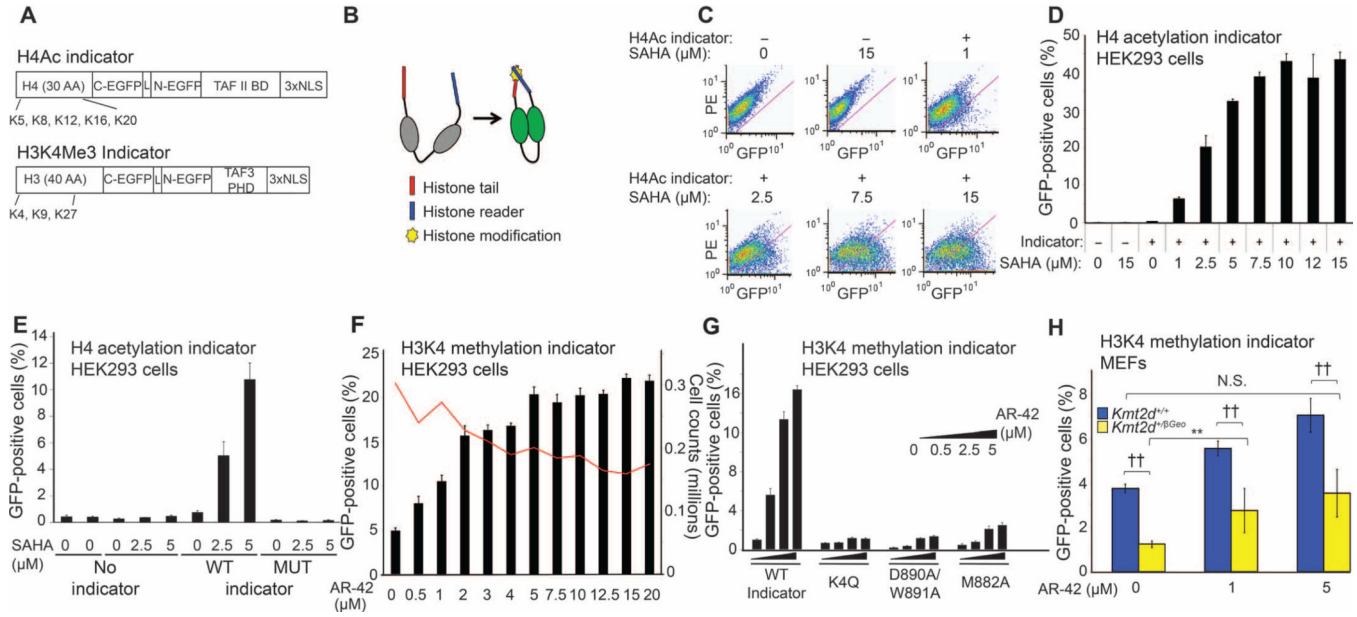

Fig. 3. H3K4me3 epigenetic reporter allele demonstrated decreased activity in *Kmt2d*$^{+/\beta Geo}$ cells

(**A**) Domain organization encoded by the H4ac and H3K4me3 reporter alleles. The H4ac indicator includes H4 (lysine positions indicated), the C- and N-terminal halves of enhanced GFP (EGFP) separated by a short linker (L), the TAFII binding domain (BD), and a repetitive nuclear localization signal (NLS). The H3K4me3 indicator includes the H3 and the TAF3-PHD. (**B**) Recognition of the histone tail mark by the relevant histone reader leads to reconstitution of GFP structure and function (fluorescence). (**C** and **D**) The acetylation indicator demonstrated increasing fluorescence with increasing amounts of the HDACi SAHA. (**E**) Activity of the H4ac indicator was lost upon mutagenesis of all potential acetylation sites from lysine to arginine. (**F**) The H3K4me3 indicator demonstrated a dose-dependent response to the HDACi AR-42 with decreased cell numbers at higher doses (red line). (**G**) Activity was greatly reduced upon mutagenesis of K4 in the H3 tail and D890A/W891A and M882A in the reader pocket. (**H**) The H3K4me3 indicator showed reduced activity in murine embryonic fibroblasts (MEFs) derived from *Kmt2d*$^{+/\beta Geo}$ mice compared to *Kmt2d*$^{+/+}$ littermates. Both genotypes showed a dose-dependent response to AR-42, with *Kmt2d*$^{+/\beta Geo}$ MEFs achieving untreated wild-type levels of activity at a dose of 5 μM. $n = 3$ (+/+), $n = 3$ (+/βGeo), biological replicates for each dose. $^{**}P < 0.01$; $^{\dagger\dagger}P < 0.001$, *t* test.

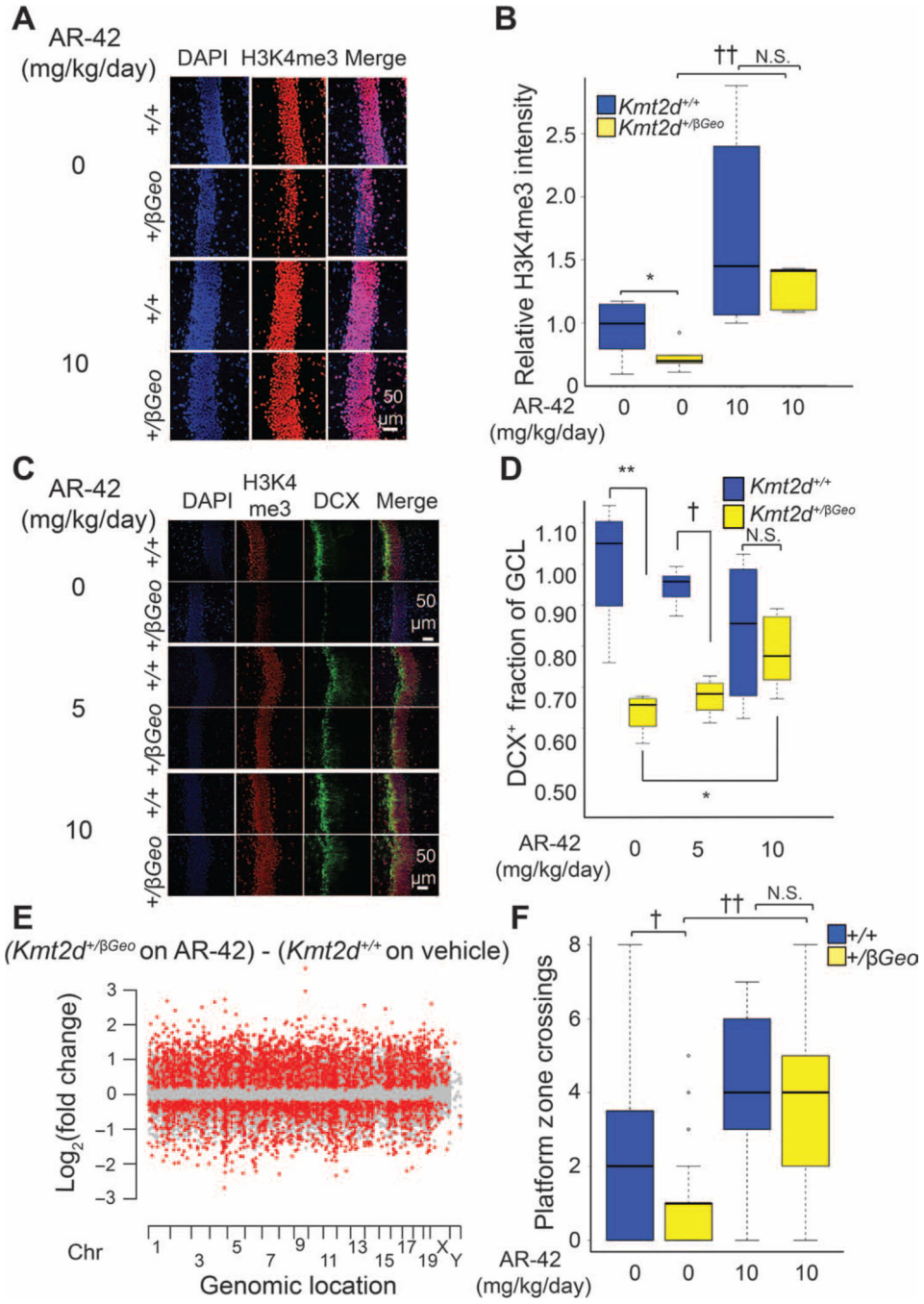

Fig. 4. In vivo effects of AR-42

(**A** to **D**) One- to 2-month-old mice of both genotypes showed an increase in H3K4me3 (**A** and **B**) (n = 5 to 6 per group) associated with a dose-dependent increase in neurogenesis in *Kmt2d*$^{+/\beta Geo}$ mice (**C** and **D**) (monitored by normalized DCX expression) (n = 4 to 6 per group) upon treatment with the HDACi AR-42. There was no difference in either H3K4me3 or neurogenesis between *Kmt2d*$^{+/\beta Geo}$ and *Kmt2d*$^{+/+}$ animals at a dose of 10 mg/kg per day. (**E**) The genome-wide deficiency of H3K4me3 seen in *Kmt2d*$^{+/\beta Geo}$ mice was improved upon treatment with AR-42 (10 mg/kg per day). (**F**) The reduced frequency of platform

crossing seen during Morris water maze testing of *Kmt2d*$^{+/\beta Geo}$ mice was normalized upon treatment with AR-42 (10 mg/kg per day) [n = 48 (+/+, no treatment), n = 32 (+/βGeo, no treatment), n = 14 (+/+, 10 mg/kg per day AR-42), n = 9 (+/βGeo, 10 mg/kg per day AR-42)]. *P < 0.05; **P < 0.01; $^{\dagger}P$ < 0.005; $^{\dagger\dagger}P$ < 0.001, t test.

Table 1

Neuropsychological findings in patients with Kabuki syndrome.

Neuropsychologic process/function	Patient 1 28 years Female	Patient 2 15 years Female	Patient 3 14 years Male
Affected gene	*KMT2D*	*KMT2D*	*KMT2D*
Full-scale IQ	87	84	66
Perceptual or nonverbal reasoning*	↓	↓	↓
Verbal reasoning/comprehension	Normal	Normal	↓
Verbal fluency*	↓	Normal	N/A
Naming*	Normal	Normal	Normal
Vocabulary/reading	Normal	Normal	N/A
Processing speed	↓	↓	↓
Basic math calculation	Normal	↓	N/A
Visual selective attention*	↓	↓	N/A
Visual working memory*	↓	↓	↓
Verbal working memory*	Normal	Normal	↓
Visual delayed memory*	↓	↓	↓
Verbal delayed memory*	↓	↓	Normal
Switching/inhibition	↓	↓	N/A
Verbal organization	Normal	Normal	N/A
Visual organization*	↓	↓	↓
Fine motor	↓	↓	↓

A retrospective analysis of neuropsychological testing on three patients with mutations in *KMT2D* revealed consistent abnormalities of functions that have been associated with the dentate gyrus. N/A, not adequately tested with used testing regimen; ↓, deficient area (defined as >1 SD below the mean and lower than full-scale IQ or, if unavailable, highest individual test score); metrics linked to the dentate gyrus are in bold font (13–15); metrics more broadly linked to the hippocampus are indicated with an asterisk (16).